On the preparatory processes of the M6.6 earthquake of June 17th, 2000, in Iceland

M. Bonafede,[1] C. Ferrari,[1] F. Maccaferri,[1] and R. Stefánsson[2]

Received 20 July 2007; revised 27 September 2007; accepted 23 November 2007; published XX Month 2007.

[1] A model is proposed to explain the spatial distribution of foreshocks of the June 17th 2000, M_s 6.6 earthquake in the South Iceland Seismic Zone (SISZ) and the high stress drop of the mainshock. Fluids of magmatic origin, ascending at near-lithostatic pressure through a low permeability layer perturb the regional stress field, inhibiting fluid flow laterally, where a high strength asperity is left. The asperity is modeled as elastic, embedded within a medium with low effective rigidity. Regional stresses due to tectonic motions are perturbed by the presence of the asperity, enhancing the production of hydrofractures and foreshocks in the NW and SE quadrants and increasing considerably the shear stress within the asperity, leading to the NS striking mainshock. **Citation:** Bonafede, M., C. Ferrari, F. Maccaferri, and R. Stefánsson (2007), On the preparatory processes of the M6.6 earthquake of June 17th, 2000, in Iceland, *Geophys. Res. Lett.*, *34*, LXXXXX, doi:10.1029/2007GL031391.

1. Introduction

[2] The South Iceland Seismic Zone (SISZ) is a left-lateral transform zone located between the Reykjanes peninsula and the east volcanic zone, with a length $L \sim 70$ km in the *EW* direction and a width $w = 10-15$ km in the *NS* direction (Figure 1). The depth h of the brittle-ductile (B-D) transition is quite sharp increasing from 8 km in the *E* to 12 km in the *W* [*Stefánsson et al.*, 1993]. The left-lateral motion is estimated by geodetic means as 1.95 cm/yr mostly in the *EW* direction [*DeMets et al.*, 1994]. One of the peculiar features of the SISZ is that the main faults are all right-lateral strike-slip and oriented *NS*, with a quite regular parallel spacing of 5–6 km, suggesting a bookshelf failure mechanism [*Einarsson*, 1991]. The historical seismicity is characterized by sequences of large earthquakes, reaching magnitude 7. A sequence lasts up to 30 years and a complete seismic cycle is ~140 years [*Stefánsson and Halldorsson*, 1988]. The mainshock of June 17th, 2000 ($M_s = 6.6$) interrupted a period of seismic quiescence since 1912. This event was followed on June 21st, 2000 by a $M_s = 6.6$ earthquake located 17 km west, which was interpreted as a triggered event [*Árnadóttir et al.*, 2003]. Migration of seismicity from east to west during short periods of time (days to weeks) is another characteristic feature of this area. The hypocenter of the June 17th, 2000 earthquake was located at 6.3 km depth and the fault surface had a length of 12.5 km along strike, oriented 7°E from *N*, and a vertical extension of 10 km (from the surface to the B-D transition), as shown by the local seismic network and by USGS and Harvard CMT solutions (R. Stefánsson et al., Earthquake prediction research and the year 2000 earthquakes in SISZ, submitted to *Bulletin of the Seismological Society of America*, 2007, hereinafter referred to as Stefánsson et al., submitted manuscript, 2007). A significant feature of the June 17th mainshock was the high magnitude w.r. to the expected magnitude for a fault with these dimensions: the average dimensions expected for the fault of a magnitude 6.6 event are 30 km length and 10 km height, with a slip of 40 cm [*Wells and Coppersmith*, 1994] while the average slip for this fault was ~2 m. This indicates a very high stress drop in the hypocentral region. The accurately located aftershocks were mostly in close proximity of the fault plane and suggest the presence of an asperity with ~3 km diameter in the middle of the fault (Figure 1c).

[3] The seismic moment release in the SISZ is in general agreement with the observed strain build up during a 140 year period [*Stefánsson and Halldorsson*, 1988]. It was also pointed out by modeling of the historical seismicity [*Roth*, 2004] that the time and place of successive earthquakes in the SISZ are not predicted by the highest induced stress, with exceptions of events very close in time and space: local strength heterogeneities seem to control the place. The two earthquakes of year 2000 released only 1/4–1/3 of the expected moment [*Árnadóttir et al.*, 2005; Stefánsson et al., submitted manuscript, 2007].

[4] In the present paper we shall focus our attention onto the foreshock activity, which shows intriguing features (described below), whose explanation may provide a better understanding of the preparatory processes of major earthquakes in the SISZ. Deep foreshocks in the area of the impending June 17th earthquake were continuous in time and nearly uniformly distributed horizontally, between ~8–10 km depth. They show magnitudes generally 1, with relatively high *b*-values 1.2 [*Wyss and Stefánsson*, 2006]. Their focal mechanisms show P-axes significantly scattered w.r. to the regional stress direction [*Lund et al.*, 2005]. Shallower foreshocks (at ~4–8 km depth) took place episodically in swarms, which became more and more frequent while approaching the time of the mainshock, and typically provided low *b*-values and P-axes coherent with the regional stress. During 9 years of sensitive micro-earthquake observations before the mainshock the spatial distribution of shallow foreshocks has been progressively concentrating within an elongated volume, oriented ~30°W of *N* and centered on the hypocenter of the impending mainshock (Figure 2).

[5] In the following sections we propose a mechanism which explains the main characteristics of deep foreshocks

[1]Department of Physics, University of Bologna, Bologna, Italy.
[2]Department of Natural Resources, University of Akureyri, Akureyri, Iceland.

0094-8276/07/2007GL031391$05.00

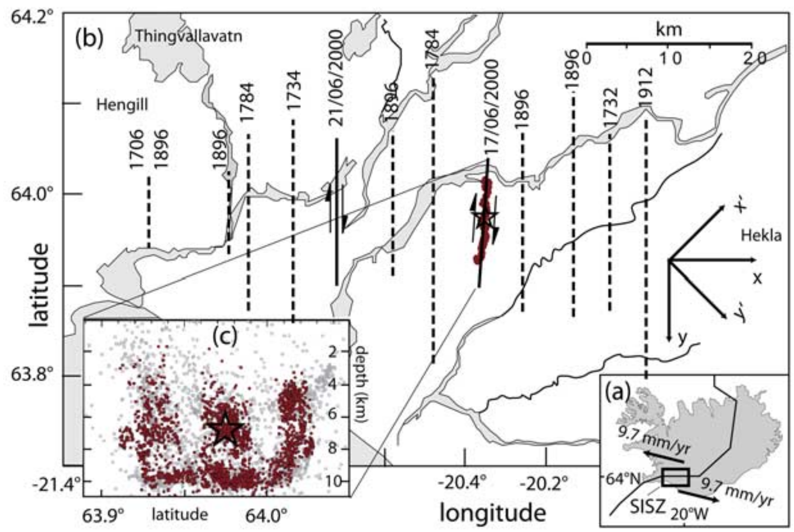

Figure 1. (a) Location of the SISZ. (b) Schematic map of historical earthquakes (dashed) and of the two mainshocks of year 2000 (solid) with reference axes x, y and x', y' employed in the text; red dots show the aftershocks on the fault plane. (c) Aftershocks of the June 17th mainshock; the lack of aftershocks between the central part of the fault and its boundaries suggests the presence of weak zones between asperities.

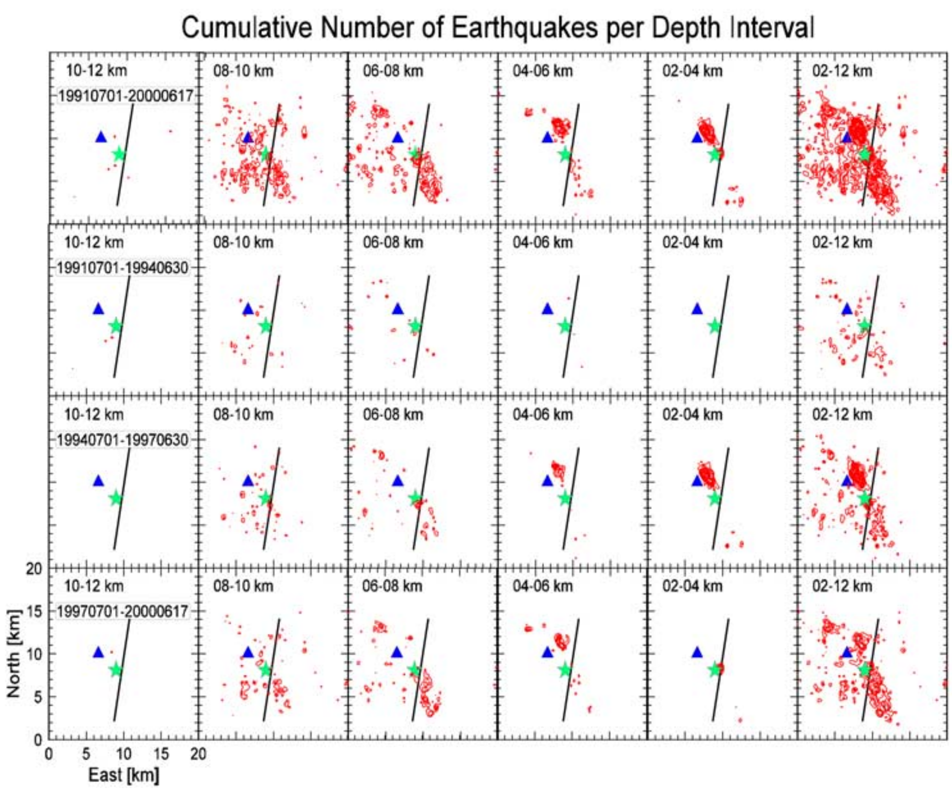

Figure 2. Foreshocks (in red) of the June 17th earthquake were clustered within a volume elongated *NW–SE*. Aftershocks, on the contrary, were sharply located within 2 km from the fault plane, striking a few degrees E of N. The green star is the epicenter of the mainshock.

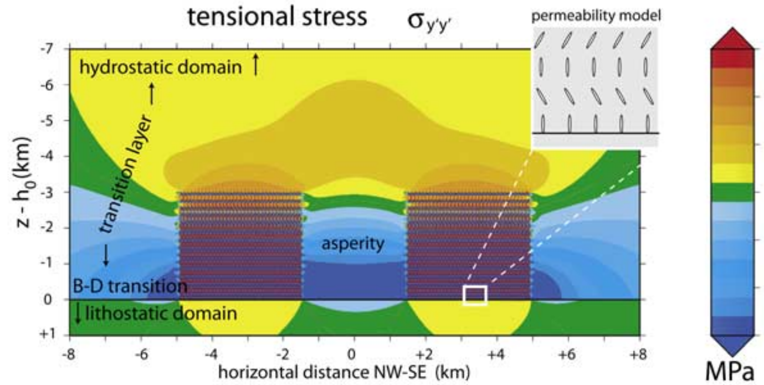

Figure 3. Stress field $\sigma_{y'y'}$, acting in the *NW–SE* direction, induced by a distribution of hydrofractures, opening above the B-D transition under the action of near-lithostatic fluid pressure. The medium below the B-D transition (modeled with effective rigidity μ_d = 10^{10} Pa) is softer than the brittle medium above (with μ_b = 3 · 10^{10} Pa). The inset shows the permeability model.

in terms of high pressure fluids ascending from the mantle and the formation of a high stress asperity.

2. High Pressure Fluids and Hydrofractures

[6] The widespread presence of fluids permeating the crust in the South Iceland Seismic zone (SISZ) was clearly demonstrated by the post-seismic deformation of the two M_s 6.6 earthquakes of June 2000 [*Jonsson et al.*, 2003]. Many evidences suggest the presence of high pressure fluids down to the base of the crust in the SISZ. Magnetotelluric data [*Hersir et al.*, 1984] indicate low resistivity (10–20 Ohm m) below the brittle-ductile transition (at 10–20 km depth). This suggests the presence of a fluid reservoir within a solid matrix. The high *b*-values of deep foreshocks is a typical feature of seismicity induced by high fluid pressure, due to the weakening role of fluids (that lower the effective normal stress) and to the pressure drop accompanying fracture extension.

[7] The presence of pressurized fluids below the B-D transition in a spreading ridge environment can be demonstrated according to the following argument. Fluids are continuously exsolved from ascending magma, due to the decreasing pressure. In the SISZ these fluids are essentially H_2O, with minor amounts of CO_2 and SO_2. In order that this water may be in mechanical equilibrium with the surrounding rock, they must be at lithostatic pressure p_0 = $\rho_r g h_0$ (where ρ_r = 2950 [kg/m^3] is rock density, g is gravity and h_0 = 10 km the depth of the B-D transition). Buoyancy forces drive these fluids upwards, toward the meteoric aquifer at hydrostatic pressure p_1 = $\rho_w g h_1$ (with ρ_w = 1000 kg/m^3, as pertinent to water in the shallow crust and h_1 = 3 km). The transition region is the layer between the lithostatic domain below h_0 and the hydrostatic domain above h_1. The fluid mass flow q_0, exsolved by the ascending plume, can be estimated as

$$q_0 = \rho_r v \epsilon \simeq 10^{-7}\ \mathrm{kg \cdot m^{-2} \cdot s^{-1}} \tag{1}$$

where v = 2–4 [cm/yr] = 0.6 · 10^{-9} [m/s] is the vertical velocity of the ascending magma, ϵ = 5% is the mass ratio of released water [*Ito et al.*, 2003]. In order that this flow may migrate according to Darcy law across the transition layer, with average permeability k_r, driven by the pressure gradient between h_0 and h_1, the permeability must be at least $k_r^{\min} = q_0\eta/(\rho_w \nabla p) \sim 5 \cdot 10^{-19}$ m^2, assuming $\rho_w \sim 500$ kg/m^3 and the fluid viscosity $\eta \sim 10^{-4}$ Pa s (pertinent to mid-crustal conditions in the SISZ).

[8] If the permeability of the transition layer is lower than $k_r^{\min}$, fluids accumulate below the B-D transition, until hydrofracture processes increase the effective permeability k_e of the deeper part of the transition layer (the high permeability commonly found at similar depths in other regions of the world is actually explained by the presence of fractures).

[9] The dependence of k_e on fluid overpressure has been modeled by *Zencher et al.* [2006] in terms of hydrofractures, employing a distribution of interacting tensile dislocations. The evolution of fluid pressure within the transition layer (h_0, h_1) can be understood in the following way: in the deeper part of the transition region, where $k_e \gg k_r$, the pressure gradient is low (according to Darcy law) so that fluids migrate at pressure values close to lithostatic; at shallower depths, fluid pressure becomes lower than the ambient horizontal stress, hydrofractures cannot open and the permeability remains at the low value k_r; the continuity of fluid flow requires that the pressure gradient is higher (in absolute value) in the shallower part of the transition layer.

3. Stress Changes Induced by Hydrofracturing

[10] The opening of several small hydrofractures (as envisaged in the effective permeability model) has non-negligible cumulative effects on the stress field: in order to evaluate such effects, we employ the solutions for the stress field due to a dislocation opening (with tensile and dip-slip components) close to the interface (the B-D transition) between two different elastic media [*Bonafede and Rivalta*, 1999; *Rivalta et al.*, 2002]. A distribution of several interacting dislocations is considered, under the effect of fluid overpressure, computed according to *Zencher et al.* [2006]. The tectonic stress field was assumed as $\sigma_{x'x'}$ = −1 MPa, compressive along *NE*, and $\sigma_{y'y'}$ = +1 MPa, tensile along *NW*. Hydrofracture planes are assumed nearly vertical (with normals in the vertical plane containing the tension axis y', inclined 0°, ±30°, w.r.t. to the horizontal, see inset of Figure 3). We consider two separate sets of dislocations, in a

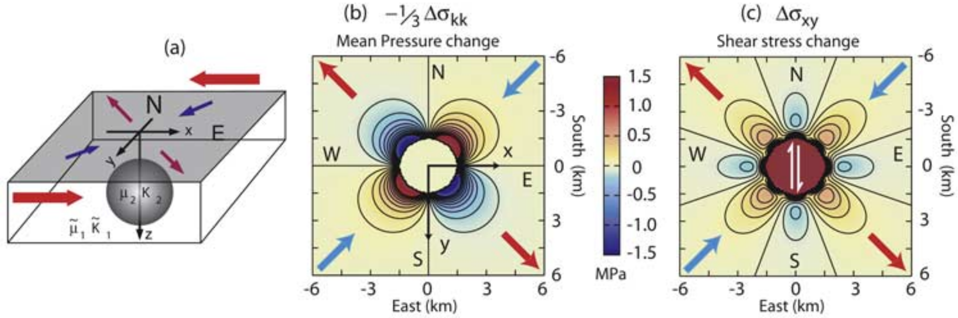

Figure 4. (a) Scheme of the asperity model. Stress induced by viscoelastic relaxation, computed on the mid-plane of the asperity: (b) the change of mean pressure induced by the asperity inhibits (enhances) the formation and opening of hydrofractures where it is positive (negative). (c) The shear stress change within the asperity is uniform, large and coherent with the tectonic field.

grid with a constant step of 100 m in both the vertical and the horizontal directions (each dislocation is 50 m long). Different arrangements were also tested, which provide very similar results.

[11] Figure 3 shows the stress component $\Delta\sigma_{y'y'}$ induced by the opening of hydrofractures; this stress component enhances fluid flow if positive, while it inhibits fluid flow if negative. The opening of hydrofractures induces compressive stresses laterally (blue areas in the Figure 3), which are larger along the harder side of the B-D transition. Above the hydrofractures, the induced stress is tensile (yellow areas), and crack opening is favored. Thus, once hydrofracturing and enhanced fluid migration starts in a region close to the B-D transition, hydrofracturing and fluid flow are inhibited in surrounding regions.

[12] We assume that seismic events obey to the modified Coulomb criterion:

$$|\tau| = S_0 + f(\sigma_n - p) \tag{2}$$

where τ is the failure stress, S_0 is the inherent rock strength, f is the coefficient of friction, σ_n is the normal stress (positive if compressive), p is the pore pressure. In the interior of a hydrofractured region, p is close to lithostatic and failure may take place at low shear stress; laterally, a high strength asperity is left, since hydrofractures are virtually absent, p is far from lithostatic and failure requires much higher stress.

[13] Another significant observation, coming from the stress map, is the presence of very variable stress inside the hydrofractured region, in agreement with the observation of heterogeneous focal mechanisms for deeper foreshocks.

4. Role of the Asperity in the Preparatory Stage

[14] A strength asperity generated by side of a hydrofractured region is modeled as an elastic spherical inclusion (at the hypocenter of the mainshock, 3 km in diameter) embedded within a medium endowed with much lower effective rigidity. The low effective rigidity may be due to at least two reasons: the hydrofractured medium is expected to be viscoelastic, owing to pressure solution processes [e.g., *Poirier*, 1985] or else the widespread presence of shear cracks (generated seismically or growing subcritically according to the stress-corrosion mechanisms) may produce low effective rigidity at large deviatoric strain [e.g., *Jaeger and Cook*, 1976, chapter 12]. In both cases, the asperity and the surrounding medium would be endowed with similar seismic velocities (sensitive to the short-term/small-amplitude elastic parameters) in agreement with seismic tomography in the SISZ [*Tryggvason et al.*, 2002]. In the following we shall focus on the viscoelastic model for the embedding medium.

[15] A sketch of the asperity model is presented in Figure 4a. A deviatoric stress field is imposed at remote distance with a compressive component (−1 MPa) in direction *SW*, and a tensile component (+1 MPa) acting *NW*. We employ *Goodier* [1933] solution for a spherical inclusion under uniform uniaxial stress and generalize it to a purely deviatoric stress configuration superposing two such solutions for two opposite uniaxial stresses acting along *NE* and *NW*. The viscoelastic (Maxwell) solution in the Laplace transform domain is obtained employing the correspondence principle, with the following substitution for the elastic parameters μ_1, K_1 of the embedding medium:

$$\widetilde{\mu_1}(s) = \frac{s\mu_1}{s + \tau^{-1}}, \qquad \widetilde{K}_1(s) = K_1 \tag{3}$$

where s is the Laplace transform variable and $\tau = \eta_1/\mu_1$ is the relaxation time (η_1 is the effective viscosity of the medium). The bulk modulus K_1 and the elastic parameters of the inclusion μ_2 and K_2 are assumed to be elastic (with $\mu_2 = \mu_1$ and $K_2 = K_1$). Finally, the stress evolution in the time domain is obtained by inverting Laplace transforms.

[16] In Figure 4b we show the change of mean pressure $-\Delta\sigma_{kk}/3$ induced by complete viscoelastic relaxation of the embedding medium. The mean pressure increases in the *NE* and *SW* quadrants, while it decreases in the *NW* and *SE* quadrants. Accordingly, the presence of the asperity inhibits hydrofracturing and increases friction in the former case, while hydrofracturing is enhanced and friction decreases in the latter. This result is consistent with the spatial distribution of shallow foreshocks (Figure 2), according to the Coulomb failure criterion (2).

[17] Finally, a significant increase of $\Delta\sigma_{xy}$ takes place inside the asperity during viscoelastic relaxation, adding 1.5 MPa to the initial 1 MPa of the deviatoric component σ_{xy} (Figure 4c). This high and uniform shear stress is consistent with the high magnitude (M_s = 6.6) and slip

(2 m) of the earthquake w.r. to the values expected from the relatively small fault dimensions.

5. Conclusions

[18] The present model explains several features of the preparatory processes leading to the M_s 6.6 earthquake of June 17th 2000 in the SISZ. A primary role is envisaged for fluids, ascending at near lithostatic pressure, from below the B-D transition. The cumulative tensile stress induced by the opening of several hydrofractures reinforces lateral variations in fluid flow and asperities are left between two high-flow regions. The different rheological behavior envisaged between an asperity and the surrounding medium perturbs further the tectonic stress, enhancing foreshock activity in selected quadrants and concentrating a high and uniform deviatoric stress within the asperity, leading to the mainshock. In the previous model the viscoelastic rheology is adopted everywhere outside the asperity; more realistically, this behavior should be restricted within bounded patches in the crust pervaded by near lithostatic fluid flow. The stress released inelastically within these patches is transferred to the elastic asperities, so that the tectonic strain may match the seismically released moment. Once a fault breaks, that region remains endowed with large permeability, the fluid pressure drops drastically and the next asperities, a few km away (Figure 3) are candidates to host the next large earthquakes. The nearly uniform interspace between consecutive faults in the SISZ may be possibly explained in this way.

[19] The present model may apply to other tectonically active areas, where fluids of deep origin are present in a low permeability crust. *Miller et al.* [2004] explain some peculiar features of the aftershocks of the 1997 Colfiorito (Italy) earthquake in terms of high pressure CO_2 released from the mantle; *Chiodini et al.* [2004] tentatively explain in a similar way the seismic activity along the Apenninic belt in Italy.

[20] **Acknowledgments.** Work performed within the 6th Framework programme of the EC (Project PREPARED). The authors gratefully acknowledge the contribution from all PREPARED participants, whose data, interpretation and ideas greatly contributed to the development of the present model. Valuable comments on the original version from two anonymous referees are gratefully acknowledged.

References

Árnadóttir, T., S. Jónsson, R. Pedersen, and G. Gudmundsson (2003), Coulomb stress changes in the South Iceland Seismic Zone due to two large earthquakes in June 2000, *Geophys. Res. Lett.*, *30*, 1205, doi:10.1029/2002GL016495.

Árnadóttir, T., S. Jónsson, F. F. Pollitz, W. Jiang, and K. L. Feigl (2005), Postseismic deformation following the June 2000 earthquake sequence in the south Iceland seismic zone, *J. Geophys. Res.*, *110*, B12308, doi:10.1029/2005JB003701.

Bonafede, M., and E. Rivalta (1999), On tensile cracks close to and across the interface between two welded elastic half-spaces, *Geophys. J. Int.*, *138*(2), 410–434, doi:10.1046/j.1365-246X.1999.00880.x.

Chiodini, G., C. Cardellini, A. Amato, E. Boschi, S. Caliro, F. Frondini, and G. Ventura (2004), Carbon dioxide Earth degassing and seismogenesis in central and southern Italy, *Geophys. Res. Lett.*, *31*, L07615, doi:10.1029/2004GL019480.

DeMets, C., R. G. Gordon, D. F. Argus, and S. Stein (1994), Effect of recent revisions to the geomagnetic reversal time scale on estimates of current plate motions, *Geophys. Res. Lett.*, *21*, 2191–2194.

Einarsson, P. (1991), Earthquakes and present-day tectonism in Iceland, *Tectonophysics*, *189*, 261–279.

Goodier, J. N. (1933), Concentration of stress around spherical and cylindrical inclusions and flaws, *J. Appl. Mech.*, *55*, A39.

Hersir, G. P., A. Björnsson, and L. B. Pedersen (1984), Magnetotelluric survey across the active spreading zone in Southwest Iceland, *J. Volcanol. Geotherm. Res.*, *20*, 253–265.

Ito, G., J. Lin, and D. Graham (2003), Observational and theoretical studies of the dynamics of mantle plume–mid-ocean ridge interaction, *Rev. Geophys.*, *41*(4), 1017, doi:10.1029/2002RG000117.

Jaeger, J. C., and N. G. W. Cook (1976), *Fundamentals of Rock Mechanics*, Chapman and Hall, London.

Jonsson, S., P. Segall, R. Pedersen, and G. Bjornsson (2003), Post-earthquake ground movements correlated to pore-pressure transients, *Nature*, *424*, 179–183, doi:10.1038/nature01776.

Lund, B., R. Slunga, and R. Bödvarsson (2005), Spatial and temporal variations of the stress field in the South Iceland seismic zone before and after the two M = 6.5 earthquakes of June 2000, *Geophys. Res. Abstr.*, *7*, 06666.

Miller, S. A., C. Collettini, L. Chiaraluce, M. Cocco, M. Barchi, and B. J. P. Kaus (2004), Aftershocks driven by a high-pressure CO_2 source at depth, *Nature*, *427*, 724–727.

Poirier, J. P. (1985), *Creep of Crystals*, 260 pp., Cambridge Univ. Press, Cambridge, U. K.

Rivalta, E., W. Mangiavillano, and M. Bonafede (2002), The edge dislocation problem in a layered elastic medium, *Geophys. J. Int.*, *149*(2), 508–523, doi:10.1046/j.1365-246X.2002.01649.x.

Roth, F. (2004), Stress changes modelled for the sequence of strong earthquakes in the South Iceland seismic zone since 1706, *Pure. Appl. Geophys.*, *161*(7), 1305–1327, doi:10.1007/s00024-004-2506-5.

Stefánsson, R., and P. Halldorsson (1988), Strain release and strain build-up in the South Iceland seismic zone, *Tectonophysics*, *159*, 267–276.

Stefánsson, R., R. Bödvarsson, R. Slunga, P. Einarsson, S. S. Jakobsdóttir, H. Bungum, S. Gregersen, J. Havskov, J. Hjelme, and H. Korhonen (1993), Earthquake prediction research in the South Iceland seismic zone and the SIL project, *Bull. Seismol. Soc. Am.*, *83*(3), 696–716.

Tryggvason, A., S. T. Rögnvaldsson, and O. G. Flovenz (2002), Three-dimensional imaging of the P- and S-wave velocity structure and earthquake locations beneath Southwest Iceland, *Geophys. J. Int.*, *151*, 848–866.

Wells, D. L., and K. J. Coppersmith (1994), New empirical relationships among magnitude, rupture length, rupture width, rupture area, and surface displacement, *Bull. Seismol. Soc. Am.*, *84*, 974–1002.

Wyss, M., and R. Stefánsson (2006), Nucleation points of recent main shocks in southern Iceland mapped by b-values, *Bull. Seismol. Soc. Am.*, *96*, 599–608.

Zencher, F., M. Bonafede, and R. Stefánsson (2006), Near-lithostatic pore pressure at seismogenic depths: A thermoporoelastic model, *Geophys. J. Int.*, *166*(3), 1318–1334.

M. Bonafede, C. Ferrari, and F. Maccaferri, Department of Physics, University of Bologna, Viale Berti-Pichat 8, I-40127 Bologna, Italy. (maurizio.bonafede@unibo.it)

R. Stefánsson, Department of Natural Resources, University of Akureyri, Borgir vid Nordurslod, 600 Akureyri, Iceland.